Extreme Mechanics Letters 72 (2024) 102223

Contents lists available at ScienceDirect

Extreme Mechanics Letters

journal homepage: www.elsevier.com/locate/eml

# A physics-informed impact model refined by multi-fidelity transfer learning

Kelsey L. Snapp [a], Samuel Silverman [b], Richard Pang [c], Thomas M. Tiano [c], Timothy J. Lawton [c], Emily Whiting [b], Keith A. Brown [a,d,e,*]

[a] Department of Mechanical Engineering, Boston University, Boston, MA, USA
[b] Department of Computer Science, Boston University, Boston, MA, USA
[c] Soldier Protection Directorate, US Army Combat Capabilities Development Command Soldier Center, Natick, MA, USA
[d] Division of Materials Science & Engineering, Boston University, Boston, MA, USA
[e] Physics Department, Boston University, Boston, MA, USA

ARTICLE INFO

*Keywords:*
Impact performance
Physics-informed model
Transfer learning
Quasistatic
Intermediate strain rate

ABSTRACT

Impact performance is a key consideration when designing objects to be encountered in everyday life. Unfortunately, how a structure absorbs energy during an impact event is difficult to predict using traditional methods, such as finite element analysis, because of the complex interactions during high strain-rate compression. Here, we employ a physics-based model to predict impact performance of structures using a single quasistatic experiment and refine that model using intermediate strain rate and impact testing to account for strain-rate dependent strengthening. This model is trained and evaluated using experiments on additively manufactured generalized cylindrical shells. Using transfer learning, the trained model can predict the performance of a new design using data from a single quasistatic test. To validate the transfer learning model, we extrapolate to new impactor masses, new designs, and a new material. The accuracy of this model allows researchers to quickly screen new designs or leverage pre-existing databases of quasistatic test data. Furthermore, when impact tests are necessary to validate design selection, fewer impact tests are necessary to identify optimal performance.

## 1. Introduction

Structures that absorb energy in impact events are critical for everyday life. They are used in bicycle helmets [1,2], the crumple zones of cars [3], packaging for shipping [4,5], and even ballistic and blast protection [6]. Despite these critical needs, development of protective impact structures is challenging because performance depends on the properties of the object to be protected, the energy of the impact, and the height and contact area of the protective structure, requiring thousands of time-consuming physical tests to optimize [10,11,7,8,9]. Further complicating the design process is that it is extremely challenging to obtain precise agreement between experiment and traditional physics-based approaches, namely finite element analysis. [12,13] Disagreement often arises due to the difficulty associated with capturing the complex interactions that occur at high strain rate, at high strain, and with self-self-contacts of the structures.

To overcome these challenges, many impact structures make use of simple bulk materials such as foams [7,14]. Such materials are simple to work with because their density can be tuned in a manner that predictably changes their performance [15]. This scaling leads to the common use of empirically measured cushion curves, which compare the peak acceleration of an impactor versus the static pressure exerted by that impactor at rest. Such cushion curves are helpful in selecting the ideal foam height and density for a given application, but assume that the height can be changed without affecting performance, limiting their applicability when applied to non-homogenous materials. Despite the widespread use of cushion curves for foams, significant research focuses on developing materials and structures that outperform foams in weight, volume, and safety metrics.

The increasing reliability and decreasing cost of additive manufacturing (AM) has opened the opportunity to manufacture structures that are more complex than traditional foams. [16,17,5] One common approach is to use AM to produce uniform lattice structures, once again depending on density scaling or repeated unit cells to predict performance [18-21]. Some researchers have investigated how structure affects performance for designs with consistent density, such as functionally grading strut thickness along an axis [22,23], auxetic structures [24,25], or using tapered beams [26]. Our previous work showed that

* Corresponding author at: Department of Mechanical Engineering, Boston University, Boston, MA, USA.
*E-mail address:* brownka@bu.edu (K.A. Brown).

https://doi.org/10.1016/j.eml.2024.102223
Received 10 July 2024; Received in revised form 15 August 2024; Accepted 18 August 2024
Available online 22 August 2024

Gaussian process regression (GPR) models could be used to predict peak acceleration of impact tests for lattice structures where the mass of the lattice is shifted between the joints and different types of struts [27]. Two promising developments are the innovation of automated testing of bulk materials to optimize impact properties [28] and the use of autonomous experiments to optimize structure for quasistatic mechanics [29,30]. Despite their promise, optimizing novel structured materials for impact performance can quickly become impractical due to the immense number of possible design choices and the burdensome testing requirements, both in researcher time and in the number of repeat samples needed for optimization.

Many efforts have been made to decrease the burden of impact testing. Early attempts focused on predicting the amount of energy that foam samples could efficiently absorb [31,32]. To account for strain-rate effects, a common strategy is to treat the material as viscoelastic or scale quasistatic curves by multiplying them by empirical constants or dynamic factors that include both strain and strain rate [33-36,9]. Recently, more numerical models have appeared to model the dynamics of impact [8,37]. Despite these efforts, little work has been done to extend these predictive models beyond homogenous foams. Facile models that accurately predict impact performance remain an open challenge.

To speed up development of new impact structures, we develop a physics-based transfer learning model to predict the ideal impact velocity $V_0^*$ for polymer structures. To explore this concept, we experimentally study generalized cylindrical shells (GCS), which have superlative energy absorbing capacity in quasistatic (QS) compression tests and are inherently easy to print using fused filament fabrication (FFF) [30]. The development of this model involves three key steps, (1) the extraction of key metrics from QS testing, (2) the use of intermediate strain rate (ISR) tests to determine strain-rate dependent strengthening, and (3) the refinement of the model using impact tests. After these initial training steps, the model is able to predict impact performance on previously unseen samples with a single QS test and even extrapolate to test data using different impactor mass, designs, and materials with an RMSE of 0.23 m/s.

## 2. Theory

An impact test consists of an impactor of mass $m$ dropping on a test component and hitting it with initial impact velocity $V_0$. The initial kinetic energy $KE$ of the impact is given by,

$$KE = \frac{1}{2} m V_0^2. \tag{1}$$

During an impact experiment, the acceleration $a$ of the impactor is tracked and used to assess the performance of the component. Typically, the impact performance of a component is defined by the maximum acceleration $a_m$ observed during the test, which should be minimized to prevent damage. However, $a_m$ is not always the clearest way to compare the performance of components as $a_m$ generally increases monotonically with $V_0$ and $m$. For ease of comparison, impact performance is often described using the non-dimensional Janssen factor $J$, which is defined as $J = a_m/a_t$ where $a_t$ is the theoretical minimum acceleration that could stop the impactor given by,

$$a_t = \frac{V_0^2}{2h}, \tag{2}$$

where $h$ is the height of the test component. While $J$ depends on the details of the impact test, namely $V_0$ and $m$, there exists a critical initial velocity $V_0^*$ for which the minimum Janssen factor $J^*$ is observed for a given $m$.

In contrast with impact tests in which the strain rate varies during the experiment, fixed-velocity tests feature a constant strain rate. Under these conditions, the useful non-dimensional metric to consider is the energy absorbing efficiency $K_s$ of a component, which describes how efficiently it absorbs energy below a force threshold $F_t$ and is given by,

$$K_s(F_t) = \frac{\int_0^{D_t} F(D)dD}{F_t h}, \tag{3}$$

with the displacement threshold $D_t$ taken as the largest $D$ for which $F(D) \leq F_t$ for all $D \leq D_t$. Practically speaking, this equation quantifies the amount of energy absorbed before exceeding $F_t$ and normalizes it by $F_t h$, which is the total amount of energy that could be absorbed if $F = F_t$ for $0 \leq D \leq h$. The maximum energy absorbing efficiency $K_s^*$ occurs at the critical force threshold $F_t^*$. Maximizing $K_s^*$ requires a long, flat plateau region, which is why most structures designed to absorb energy take advantage of productive buckling phenomenon. While there are similarities between $K_s^*$ and $J^*$, it is worth emphasizing that $K_s^*$ can be found using a single QS test while finding $J^*$ requires empirically searching for the minimum value in $V_0$ at the relevant $m$.

## 3. Results and Discussion

In order to examine the behavior of a component when impacted under various conditions, a specific GCS design was selected and fabricated out of thermoplastic polyurethane (TPU, Ninjatek – Cheetah) using FFF (Fig. 1a) and subsequently tested in impact (Fig. 1b). Representative $a$- displacement $D$ curves illustrate the outcome of testing this component with too little $KE$, an ideal amount of $KE$, and too much $KE$, all relative to the ideal conditions for this component (Fig. 1c). At low $V_0$, $a_m$ increases slowly with increasing $V_0$ due to strain-rate dependent material properties increasing the yielding force (Fig. 1d). However, once $V_0$ increases to the point where densification is reached, $a_m$ increases at a much faster rate with increasing $V_0$ as the component is unable to absorb $KE$ without densifying further. This transition point coincides with $(V_0^*, J^*)$, which is the condition under which the design is most efficient (Fig. 1e). Because of this, $(V_0^*, J^*)$ is a highly useful way to quantify impact performance. However, determining this value required a large number of impact tests on independently prepared samples and is only valid for one value of $m$.

We hypothesize that fixed-velocity tests (Fig. 1f) could be used to predict $V_0^*$. While there are substantial differences between impact and fixed-velocity testing, the move to fixed-velocity would be a tremendous reduction in the experimental burden as fixed-velocity tests use relatively common universal testing machines (UTMs), are amenable to automation, and feature fewer variables than impact tests. The result of a fixed-velocity test is a plot of force $F$ vs. $D$ (Fig. 1g). One key question in exploring our hypothesis is determining a way to extract information from this QS curve that can be useful for predicting impact performance. In analogy with the non-dimensional $J$, we consider $K_s$ (defined in Eq. (3)) as an important non-dimensional metric of a component's ability to absorb mechanical energy as previously explored by Gruenbaum, G. & Miltz [32]. Graphically, $K_s$ can be calculated by dividing the amount of energy absorbed (light blue area in Fig. 1g) while $F \leq F_t$ by the maximum amount that could be absorbed at that $F_t$ (light red area in Fig. 1g). While $F_t$ is an independent parameter that is most often chosen with consideration of the operational conditions of the component, there often exists an optimal force threshold $F_t^*$ where the component exhibits its maximum energy absorption efficiency $K_s^*$. Based on these metrics, a simple prediction of the ideal impact conditions can be found by equating impact $KE$ with the amount of energy most efficiently absorbed during QS testing,

$$\frac{1}{2} m \widetilde{V}_0^{*2} = F_t^* K_s^* h, \tag{4}$$

and then solving for predicted optimal impact velocity $\widetilde{V}_0^*$

$$\widetilde{V}_0^* = \sqrt{\frac{2F_t^* K_s^* h}{m}}. \tag{5}$$

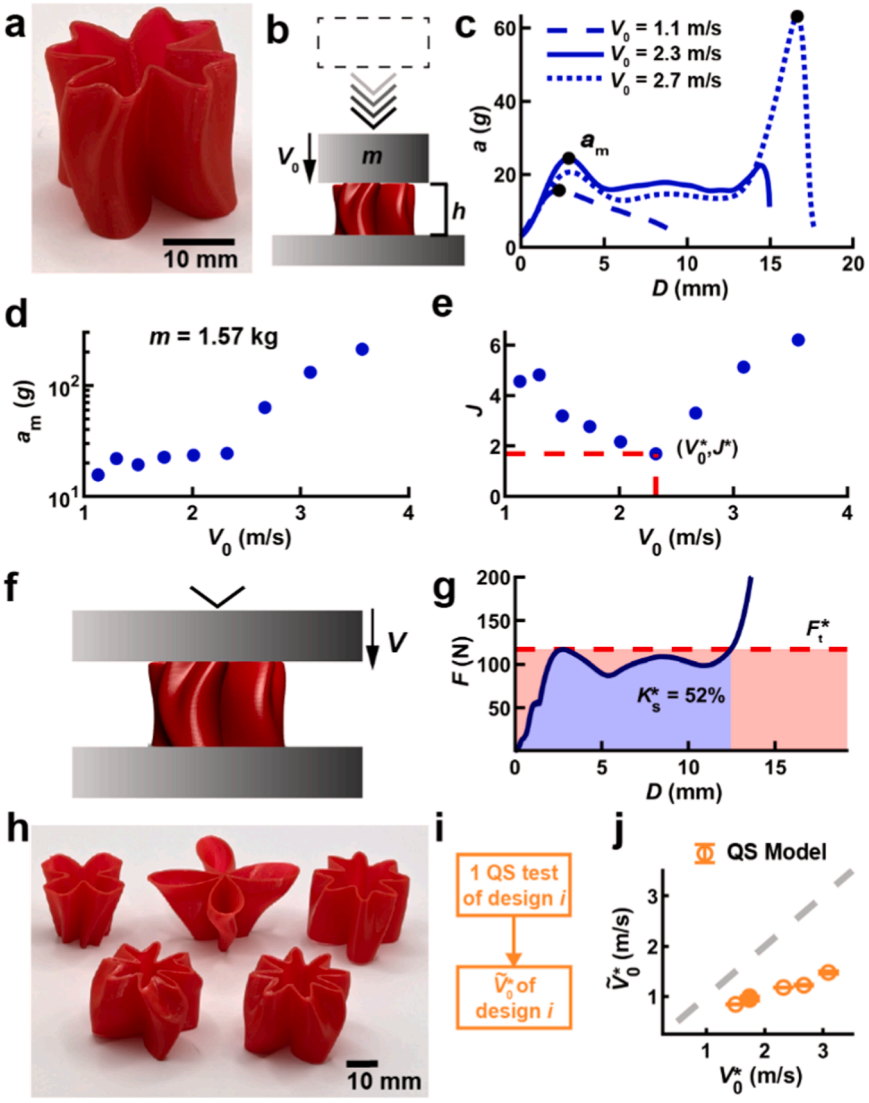


**Fig. 1.** Predicting impact performance from quasistatic tests. (a) Photograph showing a generalized cylindrical shell (GCS) component made from thermoplastic polyurethane (TPU). (b) Schematic of an impact test with impactor of mass $m$ hitting the component of height $h$ at an initial velocity $V_0$. (c) Acceleration $a$ vs. displacement $D$ for impact tests of the same component at three different $V_0$ with $m = 1.57$ kg. The max acceleration $a_m$ for each $V_0$ is denoted as a black dot. The units of $a$ are the gravitational acceleration $g$. (d) The $a_m$ at various $V_0$ with $m = 1.57$ kg. (e) Janssen factor $J$ vs. $V_0$. The test with the lowest $J$ is designated as the point $(V_0^*,J^*)$. (f) Schematic of a fixed speed test in which a platen is lowered at constant velocity $V$. (g) Force $F$ vs. $D$ for quasistatic (QS) test ($V = 2$ mm/min). This data is used to compute the most efficient operating conditions in terms of the critical force threshold $F_t^*$ and maximum mechanical energy absorbing efficiency $K_s^*$, which is defined by dividing the amount of energy absorbed (light blue area) by the maximum amount of energy that could be absorbed below $F_t^*$ (light red area). (h) Photograph showing five additional GCS designs made from TPU. (i) QS model uses a single QS test to compute the predicted optimal impactor velocity $\widetilde{V}_0^*$. (j) Parity plot showing $\widetilde{V}_0^*$ vs. $V_0^*$ for the six shown designs using the QS model for $m = 1.57$ kg. Error bars denote one standard deviation.

While the QS model is both simple and physics based, it neglects strain-rate dependent effects, which is expected to limit its predictive power.

To test the QS model, five additional designs were selected and fabricated from TPU (Fig. 1h). To apply the model, a single QS test is needed to determine $F_t^*$, $K_s^*$, and $h$ for each design. With this data, $\widetilde{V}_0^*$ for a given $m$ can be predicted using Eq. (5) (Fig. 1i). For each of the six designs, components were fabricated and tested at 2 mm/min in triplicate (Fig. 1j). While the predictions preserve rank order, they consistently underestimate $V_0^*$ because the QS model does not account for the strain-rate dependent strengthening. Despite this, because the prediction always underestimates $V_0^*$, it provides two key pieces of information. First, it provides a safe $V_0$ that will not reach densification. Second, if subsequent impact testing will be done to identify $(V_0^*, J^*)$ more accurately, it provides guidance of the lower end of potential $V_0^*$ values, potentially decreasing the number of experiments needed to identify the point of maximum performance. Nevertheless, it is clear that more information is needed to further improve this model.

In order to improve predictions of $V_0^*$, it is necessary to model the strain-rate dependent effects on the components. Using our UTM, it is possible to test at $V$ of up to 2000 mm/min (Fig. 2a). Although this is still more than an order of magnitude lower than $V_0$ during impact testing, it is several orders of magnitude higher than the 2 mm/min speed that was used in QS testing. Furthermore, when the $F$-$D$ curves are compared for these ISR tests, strain-rate dependent strengthening is readily apparent (Fig. 2b). Specifically, the curves have similar shapes, but $F$ increases with increasing $V$. Interestingly, higher $V$ has a modest effect on $K_s^*$ (Fig. 2c), which bears the advantage that QS tests can be used to estimate this value. In contrast, $F_t^*$ monotonically increases with increasing $V$ (Fig. 2d), making this parameter a clear quantification of strain-rate dependent strengthening. Empirically, we find that these experiments

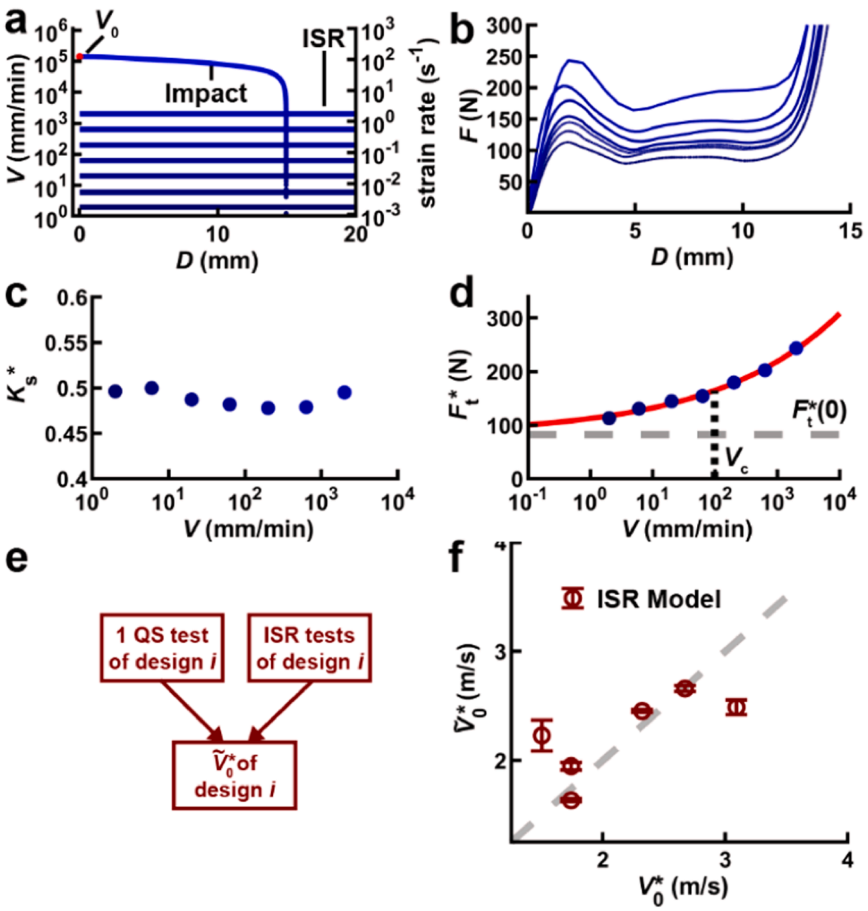


**Fig. 2.** Predicting impact performance from intermediate strain rate tests. (a) Velocity $V$ vs. $D$ during impact and intermediate strain rate (ISR) tests. While impact tests start at $V = V_0$ and decrease as energy is absorbed, ISR tests have a fixed $V$ for the entire test. (b) $F$ vs. $D$ for ISR tests of copies of the component shown in Fig. 1a. (c) $K_s^*$ vs. $V$ for the ISR tests shown in b. (d) $F_t^*$ vs. $V$ for the ISR tests shown in b. The red line shows a fit to Eq. (6) with key fitting constants $F_t^*(0)$ and $V_c$ marked by gray and black dashed lines, respectively. (e) ISR model uses both QS and ISR tests of the target design to predict $\widetilde{V}_0^*$. (f) Parity plot showing $\widetilde{V}_0^*$ vs. $V_0^*$ for the six original designs using the ISR model for $m = 1.57$ kg. Error bars denote one standard deviation. In panels a, b, c, and d, shades of blue indicate $V$.

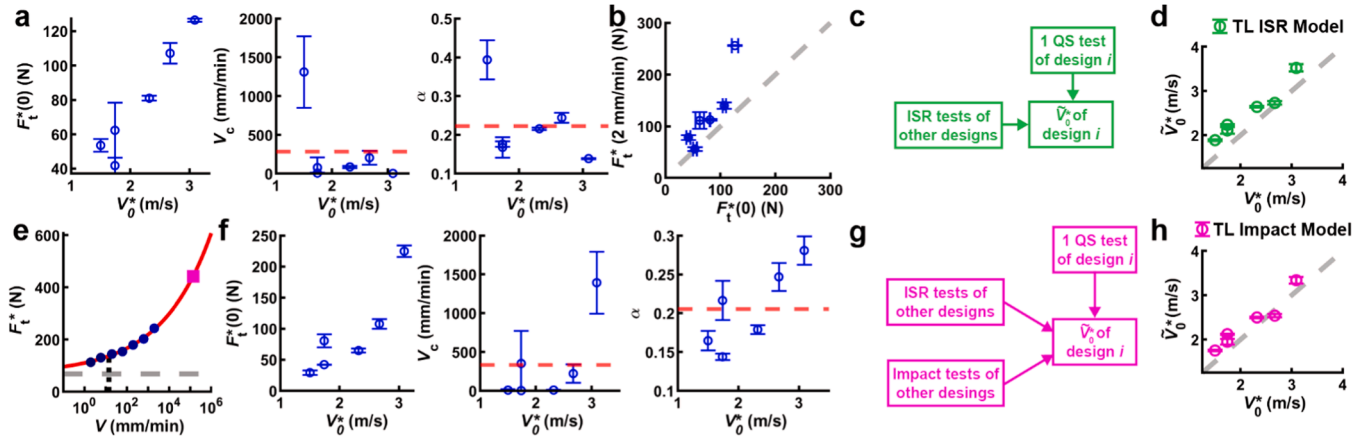


**Fig. 3.** Predicting impact performance using transfer learning. (a) Values from ISR fitting each of the six designs to Eq. (6) with the mean value shown as a dashed red line. (b) Plot of QS $F_t^*(2$ mm/min) vs. fitting constant $F_t^*(0)$. (c) Transfer learning (TL) ISR model that uses ISR tests of other designs to calculate $V_c$ and $\alpha$, allowing the prediction of $\widetilde{V}_0^*$ with a single QS test for each target design. (d) Parity plot showing $\widetilde{V}_0^*$ vs. $V_0^*$ for the six designs using the TL ISR model for impactor mass $m = 1.57$ kg using leave-one-out cross validation (LOOCV) to calculate $V_c$ and $\alpha$ for each prediction. (e) $F_t^*$ vs. $V$ for ISR tests with theoretical impact point $(V_0^*, F_t^*)$ (pink square) calculated using Eq. (7). (f) Values from ISR and impact fitting each of the six designs to Eq. (6) with the mean value shown as dashed red line. (g) TL impact model uses ISR tests and impact $F_t^*$ prediction from other designs to calculate parameters $V_c$ and $\alpha$, allowing the prediction of $\widetilde{V}_0^*$ with just a single QS test for each new target design. (h) Parity plot of $\widetilde{V}_0^*$ vs. $V_0^*$ for the six original designs using the TL impact model for $m = 1.57$ kg using LOOCV. Error bars throughout represent one standard deviation.

can be fit using,

$$F_t^*(V) = \quad F_t^*(0)\left(1+\left(\frac{V}{V_c}\right)^{\alpha}\right), \tag{6}$$

with fitting constants $F_t^*(0)$, $V_c$, and $\alpha$. These fitting constants have a physical basis: $F_t^*(0)$ represents the asymptotic limit of $F_t^*$ for ISR testing when $V$ approaches 0, $V_c$ represents the characteristic velocity where $F_t^*(V)$ doubles, and $\alpha$ represents how quickly $F_t^*(V)$ increases as $V$ increases. The ISR model is formed by combining Eq. (6) and Eq. (5) to obtain a transcendental equation that can be solved numerically to predict $\widetilde{V}_0^*$ of a given design based upon QS and ISR tests for the design (Fig. 2e). The predictive performance of the ISR model is significantly improved, although the rank order is no longer correct (Fig. 2f). Despite this improvement, the ISR model only uses data from a given design and requires a large number of fixed velocity tests for each prediction.

Despite the improvements with the ISR model, taking a full sweep of ISR test data is much slower than taking a single QS test and high-speed tests have the potential to damage the load cells of UTMs. Therefore, we hypothesized that transfer learning could be employed to eliminate the need to take ISR tests for each new target design. By plotting the fitting constant values for $F_t^*(0)$, $V_c$, and $\alpha$, some trends become clear (Fig. 3a). While $F_t^*(0)$ clearly varies for each design, both $V_c$ and $\alpha$ have more closely grouped values for all tested designs, suggesting that their mean values could be used. Fortunately, $F_t^*(0)$ is correlated with $F_t^*(2$ mm/min) determined by QS experiments of the target design (Fig. 3b). Therefore, a transfer learning model can be created that uses the mean value of $V_c$ and $\alpha$ from other designs while establishing $F_t^*(0)$, $K_s^*$, and $h$ from a single QS test (Fig. 3c) for each new target design. In this way, the time-consuming ISR tests can be done once for a representative set of designs to establish baseline values, and then subsequent designs can be predicted using a single QS test. Interestingly, when predicting impact performance using leave-one-out cross validation (LOOCV), the new TL ISR model performs significantly better than the ISR model trained on ISR data from each target point (Fig. 3d). This suggests that $V_c$ and $\alpha$ are not design dependent, as averaging the values for several designs provides better predictive performance than using the value from the specific design.

Motivated by the success of incorporating ISR data from other designs, we hypothesized that using limited impact testing could further improve the prediction of $F_t^*(V)$. Unfortunately, impact tests do not produce an estimate of $F_t^*$ that can be directly used to estimate strain-rate dependent strengthening at these higher strain rates. Despite this, the value of $V_0^*$ determined by impact experiments for each design can be used to compute what the required $F_t^*(V)$ would need to have been to arrive at the correct prediction, which can be computed by rearranging Eq. (4) as,

$$F_t^*(V_0^*) = \frac{mV_0^{*2}}{2K_s^*h}. \tag{7}$$

This $(V_0^*, F_t^*(V_0^*))$ point can then be included in the $F_t^*(V)$ fit model to further improve its accuracy at high velocities (Fig. 3e). Fitting the ISR and impact data together to Eq. (6), we find that the additional point provided by impact testing barely changes $F_t^*(0)$, but slightly adjusts $V_c$ and $\alpha$ (Fig. 3f). Importantly, the scaling parameter $\alpha$ decreases from 0.223 to 0.205, suggesting that the TL ISR model overestimates the strain-rate dependent strengthening at higher velocities. With this addition, the TL impact model can predict $\widetilde{V}_0^*$ using a model initialized on a representative set of ISR and impact tests and a single QS test for each new design (Fig. 3g). The TL impact model shows slight improvements to predictive accuracy at the cost of including some impact data to train the initial model (Fig. 3h). The similarities between the results shown in Figs. 3d and 3h demonstrate that including the impact results merely refines the TL ISR model from what is possible when including ISR testing alone, which is further supported by the modest adjustments to the fitting parameters $V_c$ and $\alpha$ with the inclusion of the impact data.

To further explore the transferability of this model, we tested two new designs at $m = 3.1$ kg, nearly twice the mass of the impactor used to generate all training data. The first design (Fig. 4a) had low stiffness and no clearly defined yield point (Fig. 4b). All models predict the very low $\widetilde{V}_0^*$ for this soft design, consistent with the test data obtained from impact testing (Fig. 4c). In contrast, another design (Fig. 4d) was chosen that had a higher $F_t^*$ than previous designs and a clear yielding region (Fig. 4e). Here, the models predict higher $\widetilde{V}_0^*$ consistent with experimental results, with the QS model being the notable outlier because it fails to account for the strain-dependent strengthening of the material that is amplified by this stiff design (Fig. 4f).

As a final test of generalizability, we extended these models to a new material, a TPU filament mixed with a blowing agent (ColorFabb – VarioShore) such that when printed at 250 °C, it forms a foam with a density half of the previously studied TPU. When testing solid cylinder samples fabricated with both the TPU and foaming TPU (Fig. 5a), the foaming TPU sample shows a significantly lower modulus and densifies at a much higher strain due to the added porosity from the blowing agent decreasing the relative density of the material at the microstructural scale. Furthermore, we switched to a more complex GCS design space (Fig. 5b), which adds a tapered region to provide an initial region with low stiffness. Some of the new foaming TPU designs had heights that included those much lower than the previously studied designs and some were up to twice the mass of any components in the training set (Fig. 5c). The new designs generally had much lower $K_s^*$ due to the inefficiency of the tapered region (Fig. 5d), but they also had much higher $F_t^*$, which were designed to target higher $V_0^*$. All four models were applied to the 14 new foaming TPU designs, with both TL models' $V_c$ and $\alpha$ parameter values being trained exclusively on data from the original six TPU designs. The TL impact model had an RMSE of 0.23 m/s, with the TL ISR model close behind and the ISR and QS models' errors significantly higher (Fig. 5e). The TL impact model trained exclusively on the original six TPU data shows excellent accuracy at predicting impact performance using only a single QS test for each new foaming TPU design (Fig. 5f), especially considering that the design space, $h$, component mass, and component material were all broadened from those contained in the training data. This suggests that the physics-informed transfer learning model may be able to extrapolate far beyond the limited training data used to train it.

## 4. Conclusion

This work reports a systematic exploration of how the impact performance of structures can be predicted using a set of models with varying complexity. In all cases, models are physics informed to meaningfully connect metrics from QS testing to impact performance. Our key finding is that the incorporation of related training data that includes testing in the ISR and impact regimes allows these models to powerfully extrapolate to new designs, materials, and impact conditions. From a design perspective, this work implies that once a representative set of data has been acquired, new designs can be rapidly evaluated based on a single QS test. Furthermore, the success of this model in extrapolating beyond the training materials suggests that models trained on large databases of polymeric structures may be useful with new materials and architectures. To that end, the TL impact model based on all data presented in this study is given by $V_c = 331$ mm/min and $\alpha = 0.205$, which, when combined with a single QS test of a new sample, can be used to estimate $\widetilde{V}_0^*$.

The ability to predict performance with a single QS test allows researchers to screen candidate structures for impact performance quickly and easily. Additionally, it allows researchers to leverage databases of QS tests already published or that can be generated using high throughput experimentation or self-driving labs. Finally, researchers can take advantage of previously studied design motifs, such as how the

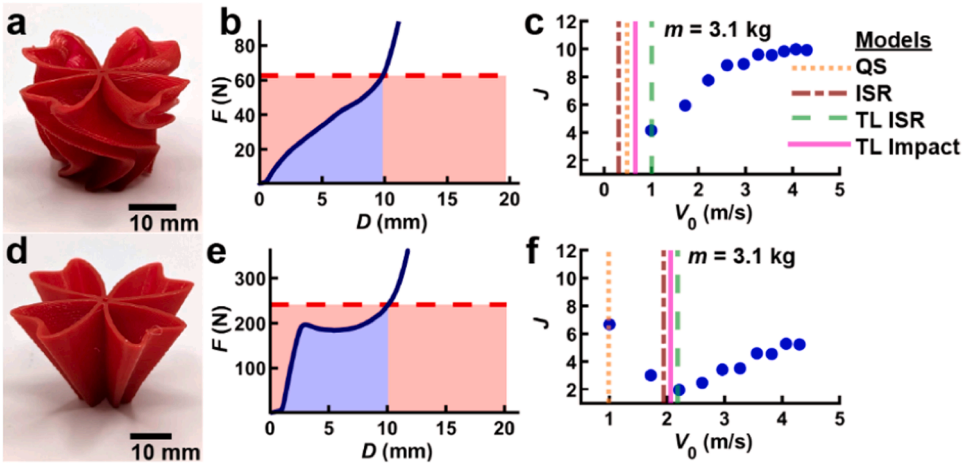


**Fig. 4.** Validation testing with new designs and a larger impactor mass. (a) New design printed from TPU. (b) QS test for new design showing $F$ vs. $D$ with red dashed line indicating $F_t^*$. (c) $J$ vs. $V_0$ for the design shown in a with $m = 3.1$ kg. Dashed lines represent $\widetilde{V}_0^*$ using the four models with color denoting the model. (d) Second new design printed from TPU. (e) QS test for second new design showing $F$ vs. $D$ with red dashed line indicating $F_t^*$. (f) Values of $J$ vs. $V_0$ for design shown in d for $m = 3.1$ kg. Dashed lines represent $\widetilde{V}_0^*$ using the four models with color denoting the model.

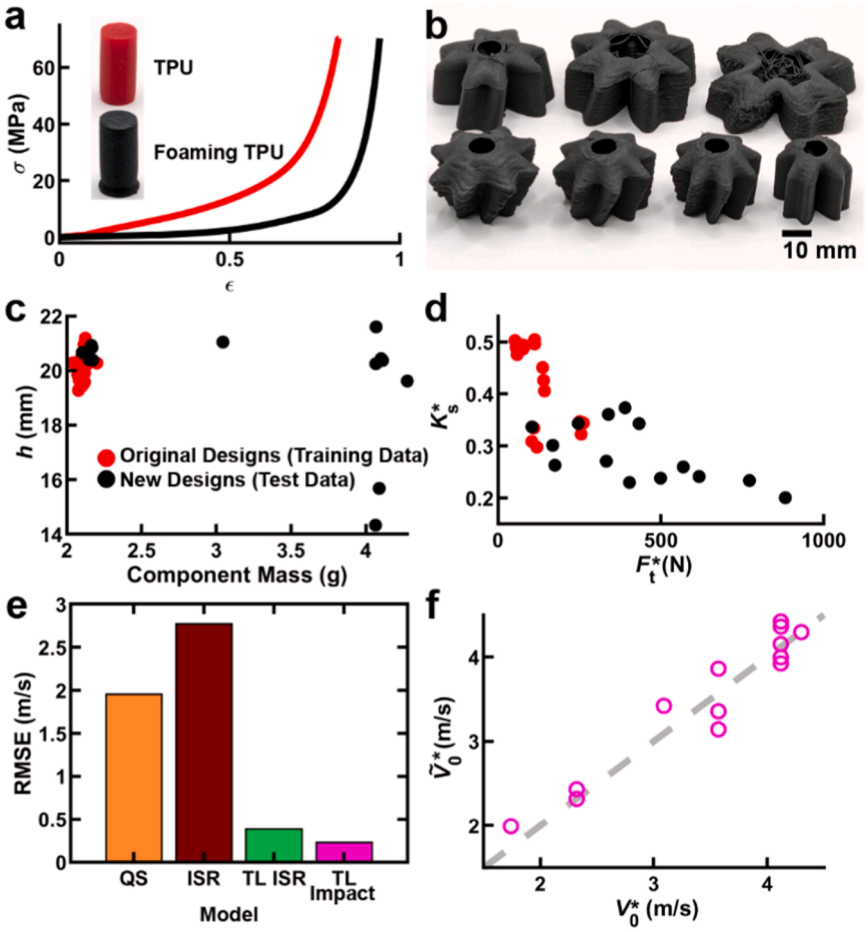


**Fig. 5.** Extending transfer learning models to an additional material. (a) Stress $\sigma$ vs. strain $\epsilon$ for QS tests of solid cylinders 8 mm in diameter with $h = 16$ mm for material characterization. (b) Picture of seven of the 14 additional designs fabricated with a foaming TPU filament. (c) The $h$ vs. component mass for original six designs and the new 14 foaming TPU designs. (d) The $K_s^*$ vs. $F_t^*$ for original six designs and new 14 foaming TPU designs. (e) Root mean squared error (RMSE) for predictions of $V_0^*$ of new foaming TPU designs. Both TL models use fitting constants $V_c$ and $\alpha$ trained solely on data from original six TPU designs. (f) Parity plot showing $\widetilde{V}_0^*$ vs. $V_0^*$ for the 14 foaming TPU designs using the TL Impact model for $m = 1.57$ kg.

angle, aspect ratio, or connectivity of lattices affect their force-displacement response, to predict their impact performance. [12,38,39] When impact testing is required to validate a chosen design, knowing the $\widetilde{V}_0^*$ before impact testing can significantly decrease the number of tests needed to pinpoint $(V_0^*, J^*)$. Furthermore, by using a physics-informed model instead of density or other approaches that depend on the specific structure of the individual design or material, it is more likely that the model will extrapolate to more disparate designs and structures.

By examining Eq. 5, it is possible to understand what properties are necessary for good impact performance. First, increasing the $h$ of the component directly translates into improved impact performance, so the component should take advantage of as much vertical space as is feasible within design constraints. Second, the $K_s^*$ is directly correlated with impact performance. Because $K_s^*$ is found to be tolerant to strain-rate dependent effects, QS testing can be used to identify high performance designs with long, flat plateau regions. Finally, $F_t^*$ affects impact performance. However, $F_t^*$ is often limited by the fragility of the object to be protected and therefore usually must be optimized in coordination with the design objectives of the system as a whole.

## 5. Methods

GCS designs consist of 11 parameters that transform a standard cylindrical shell [30]. The STLs were generated using a previously published python script [40]. For foaming TPU designs, tapered regions were added to the GCS components by adding two distinct regions in the axial direction. First, there is a transition zone where the top shape of the GCS component increases in diameter while the lobes are decreased in size. The second region transforms the intermediate shape to a circular cross section with a small diameter, creating a reentrant region that can collapse into itself while offering low stiffness. These modifications retain the topological nature of the GCS space and can be considered a subset of GCS.

The STLs were converted into gcode using Slic3r using spiral vase mode and sent to the printers using Octoprint. Components were printed on one of five MakerGear M3-ID FFF printers on a glass bed covered with polyimide tape with 0.75 mm nozzles. Components were printed using either TPU (Ninjatek - Cheetah) or foaming TPU (ColorFabb - VarioShore) filament. Components were printed at 250 °C nozzle temperature and 80 °C bed temperature. The bed was heated to 100 °C before removal.

Components were removed from the printers using a UR5e (Universal Robotics) 6-axis robot arm and transferred to a scale (Sartorius CP225D) to record the mass. Afterwards, components for impact testing were placed on a table by the robot arm for temporary storage. Components for QS or ISR testing were moved by the robot to a UTM (Instron 5965). QS tests for each design were performed at 2 mm/min until the force reached 4.5 kN. A single ISR test for each design was performed at each speed (6, 20, 63, 200, 632, or 2000 mm/min). For higher testing speeds, the 4.5 kN threshold was lowered for some designs that densify quickly to protect the UTM from damage, but this did not prevent the proper calculation of $K_s^*$ or $F_t^*$. For TPU, QS tests were performed in triplicate while single QS tests were performed for each foaming TPU design. Components tested in impact were transferred to another location for testing on a drop tower impact system (Ceast 9350) with a flat-ended steel impactor with a mass of either 1.57 or 3.1 kg. Because impact testing took place at an alternate site, there was an interval of several days between fabrication and testing of impact components.

QS and ISR tests record data as $F$-$D$ data. The $h$ of the component is calculated by measuring when the $F$ first reaches 1 N. The $K_s^*$ and $F_t^*$ are then found by calculating the max and argmax of Eq. (3). For impact testing, each design is tested once at each $V_0$. Impact data is recorded as $a$ vs. time. Because of noise in the signal, $a$ is smoothed using a Gaussian filter by using the MATLAB function "smoothdata" with a smoothing factor of 0.13. The $a_m$ is then taken as the max of this smoothed curve. Subsequently $V_0^*$ and $J^*$ are calculated by finding the minimum $J$ for each design and its corresponding $V_0$.

When calculating $\widetilde{V}_0^*$, only a single QS test was used at a time. Therefore, to get standard deviation for the TPU models, the models were rerun with each of the three QS experiments. Likewise, when fitting Eq. (6), a single QS test was paired with all ISR tests for each of the three predictions using the MATLAB function "fit" with the restriction that of $F_t^*(0) \geq 0$, $V_c \geq 2$ mm/min, and $\alpha \geq 0$. For LOOCV predictions (Fig. 3), ISR data from the target design was excluded when calculating the mean of fitting constant $V_c$ and $\alpha$. However, fitting constant $F_t^*(0)$ was calculated from the $F_t^*$ of the single QS test used for each of the three predictions for that design. When predicting $\widetilde{V}_0^*$ for the new designs (Fig. 4c,f and Fig. 5), ISR data from all six original TPU designs were used when calculating the mean of fitting constants $V_c$ and $\alpha$. Only a single QS experiment was performed for each foaming TPU design, so no standard deviation was reported.

## CRediT authorship contribution statement

**Kelsey L Snapp:** Writing – review & editing, Writing – original draft, Software, Investigation, Formal analysis, Data curation, Conceptualization. **Samuel Silverman:** Writing – review & editing, Software. **Thomas M Tiano:** Writing – review & editing, Conceptualization. **Richard Pang:** Writing – review & editing, Investigation. **Emily Whiting:** Writing – review & editing, Supervision, Conceptualization. **Timothy J. Lawton:** Writing – review & editing, Supervision, Investigation, Conceptualization. **Keith Brown:** Writing – review & editing, Writing – original draft, Supervision, Conceptualization.

## Declaration of Competing Interest

The authors declare no competing financial interests.

## Data availability

All data is available at https://open.bu.edu/handle/2144/46509.

## Acknowledgements

This work was supported by the National Science Foundation (CMMI-1661412 and DMR-2323728) and the US Army CCDC Soldier Center (contract W911QY2020002).

## References

[1] S.V. Caswell, T.E. Gould, J.S. Wiggins, Protective helmets in sports, Mater. Sports Equip. (2007) 87–126, https://doi.org/10.1533/9781845693664.1.87.
[2] E.C. Clough, et al., Elastomeric microlattice impact attenuators, Matter 1 (2019) 1519–1531.
[3] V. Lukoševičius, D. Juodvalkis, A. Keršys, R. Makaras, Investigation of functionality of vehicle crumple zones recovered after a traffic accident, Appl. Sci. 13 (2023).
[4] C. Ge, D. Cormier, B. Rice, Damping and cushioning characteristics of Polyjet 3D printed photopolymer with Kelvin model, J. Cell. Plast. vol. 57 (2021) 517–534.
[5] M.K. Thompson, et al., Design for additive manufacturing: trends, opportunities, considerations, and constraints, CIRP Ann. - Manuf. Technol. 65 (2016) 737–760.
[6] F. Zhu, G. Lu, D. Ruan, Z. Wang, Plastic deformation, failure and energy absorption of sandwich structures with metallic cellular cores, Int. J. Prot. Struct. 1 (2010) 507–541.
[7] M. Tomin, M.Á. Lengyel, R.D. Párizs, Á. Kmetty, Measuring and mathematical modeling of cushion curves for polymeric foams, Polym. Test. 117 (2023).
[8] J.M. Gibert, G.S. Batt, Impact oscillator model for the prediction of dynamic cushion curves of open cell foams, Packag. Technol. Sci. vol. 28 (2015) 227–239.
[9] G. Li, V. Rouillard, M.A. Sek, Evaluation of static and dynamic cushioning properties of polyethylene foam for determining its cushion curves, Packag. Technol. Sci. vol. 28 (2015) 47–57.
[10] C. Ge, H. Huang, Corner foam versus flat foam: an experimental comparison on cushion performance, Packag. Technol. Sci. vol. 28 (2015) 217–225.
[11] C. Ge, Theory and practice of cushion curve: a supplementary discussion, Packag. Technol. Sci. vol. 32 (2019) 185–197.

[12] M. Smith, Z. Guan, W.J. Cantwell, Finite element modelling of the compressive response of lattice structures manufactured using the selective laser melting technique, Int. J. Mech. Sci. 67 (2013) 28–41.
[13] M. Helou, S. Vongbunyong, S. Kara, Finite element analysis and validation of cellular structures, Procedia CIRP 50 (2016) 94–99.
[14] V.S. Deshpande, N.A. Fleck, High strain rate compressive behaviour of aluminum alloy foams, Int. J. Impact Eng. 24 (2000) 277–298.
[15] J. Zhang, M.F. Ashby, Mechanical selection of foams and honeycombs used for packaging and energy absorption, J. Mater. Sci. 29 (1994) 157–163.
[16] D.J. Roach, et al., Utilizing computer vision and artificial intelligence algorithms to predict and design the mechanical compression response of direct ink write 3D printed foam replacement structures, Addit. Manuf. 41 (2021) 101950.
[17] G.S. Ganitano, S.G. Wallace, B. Maruyama, G.L. Peterson, A hybrid metaheuristic and computer vision approach to closed-loop calibration of fused deposition modeling 3D printers, Prog. Addit. Manuf. 9 (2024) 767–777.
[18] C. Ling, A. Cernicchi, M.D. Gilchrist, P. Cardiff, Mechanical behaviour of additively-manufactured polymeric octet-truss lattice structures under quasi-static and dynamic compressive loading, Mater. Des. 162 (2019) 106–118.
[19] M.C. Messner, Optimal lattice-structured materials, J. Mech. Phys. Solids 96 (2016) 162–183.
[20] J.A. Hawreliak, et al., Dynamic behavior of engineered lattice materials, Sci. Rep. 6 (2016) 1–7.
[21] A.P. Garland, et al., Deep convolutional neural networks as a rapid screening tool for complex additively manufactured structures, Addit. Manuf. 35 (2020) 101217.
[22] J.J. Andrew, J. Ubaid, F. Hafeez, A. Schiffer, S. Kumar, Impact performance enhancement of honeycombs through additive manufacturing-enabled geometrical tailoring, Int. J. Impact Eng. 134 (2019) 103360.
[23] D.S.J. Al-Saedi, S.H. Masood, M. Faizan-Ur-Rab, A. Alomarah, P. Ponnusamy, Mechanical properties and energy absorption capability of functionally graded F2BCC lattice fabricated by SLM, Mater. Des. 144 (2018) 32–44.
[24] S. Yuan, C.K. Chua, K. Zhou, 3D-printed mechanical metamaterials with high energy absorption, Adv. Mater. Technol. vol. 4 (2019).
[25] R.P. Bohara, S. Linforth, T. Nguyen, A. Ghazlan, T. Ngo, Novel lightweight high-energy absorbing auxetic structures guided by topology optimisation, Int. J. Mech. Sci. 211 (2021) 106793.
[26] T. Tancogne-Dejean, D. Mohr, Stiffness and specific energy absorption of additively-manufactured metallic BCC metamaterials composed of tapered beams, Int. J. Mech. Sci. 141 (2018) 101–116.
[27] A.E. Gongora, et al., Designing lattices for impact protection using transfer learning, Matter 5 (2022) 2829–2846.
[28] M. Hernández-del-Valle, et al., Robotically automated 3D printing and testing of thermoplastic material specimens, Digit. Discov. 2 (2023) 1969–1979.
[29] A.E. Gongora, et al., A Bayesian experimental autonomous researcher for mechanical design, Sci. Adv. 6 (2020).
[30] K.L. Snapp, et al., Superlative mechanical energy absorbing efficiency discovered through self-driving lab-human partnership, Nat. Commun. 15 (2024) 4290.
[31] T. Ansorge, K. Nendel, Calculation of cushion diagrams using a physical model, Packag. Technol. Sci. 11 (1998) 1–9.
[32] G. Gruenbaum, J. Miltz, Static versus dynamic evaluation of cushioning properties of plastic foams, J. Appl. Polym. Sci. 28 (1983) 135–143.
[33] H.J. Qi, M.C. Boyce, Stress-strain behavior of thermoplastic polyurethanes, Mech. Mater. 37 (2005) 817–839.
[34] Y. Miao, H. He, Z. Li, Strain hardening behaviors and mechanisms of polyurethane under various strain rate loading, Polym. Eng. \ Sci. 60 (2020) 1083–1092.
[35] M.A. Sek, M. Minett, V. Rouillard, B. Bruscella, A new method for the determination of cushion curves, Packag. Technol. Sci. vol. 13 (2000) 249–255.
[36] O. Ramon, J. Miltz, Prediction of dynamic properties of plastic foams from constant–strain rate measurements. J. Appl. Polym. Sci. 40 (1990) 1683–1692.
[37] A. Joodaky, G.S. Batt, J.M. Gibert, Prediction of cushion curves of polymer foams using a nonlinear distributed parameter model, Packag. Technol. Sci. vol. 33 (2020) 3–14.
[38] X. Chen, et al., Adjusting unit cell three-dimensional posture and mirror array: a novel lattice structure design approach, Mater. Des. 221 (2022) 110852.
[39] R. Liu, W. Chen, J. Zhao, A review on factors affecting the mechanical properties of additively-manufactured lattice structures, J. Mater. Eng. Perform. 33 (2024) 4685–4711.
[40] Silverman, S. bu-shapelab/gcs: v1.2.3. https://doi.org/10.5281/zenodo.10933597 (2024).